Geophysical Research Letters

RESEARCH LETTER
10.1029/2023GL103019

Theoretical Study of Interhemispheric Electron Bouncing Within Pulsating Aurora

George V. Khazanov[1], Mike Chu[2], Marilia Samara[1], and Robert G. Michell[1]

[1]NASA Goddard Space Flight Center, Greenbelt, MD, USA, [2]The Space Weather Lab, George Mason University, Fairfax, VA, USA

Key Points:

- Modeling of the time-dependent formation of the electron precipitation dynamics affiliated with the region of pulsating aurora
- A quantitative assessment of the role of atmospheric collisions in electron precipitation phenomena within the pulsating aurora

Correspondence to:

G. V. Khazanov,
George.V.Khazanov@nasa.gov

Citation:

Khazanov, G. V., Chu, M., Samara, M., & Michell, R. G. (2023). Theoretical study of interhemispheric electron bouncing within pulsating aurora. *Geophysical Research Letters*, *50*, e2023GL103019. https://doi.org/10.1029/2023GL103019

Received 25 JAN 2023
Accepted 13 APR 2023

Author Contributions:

Conceptualization: George V. Khazanov
Data curation: George V. Khazanov, Marilia Samara, Robert G. Michell
Formal analysis: George V. Khazanov
Investigation: George V. Khazanov
Methodology: George V. Khazanov
Resources: George V. Khazanov
Software: George V. Khazanov
Supervision: George V. Khazanov
Validation: George V. Khazanov
Visualization: Mike Chu
Writing – original draft: George V. Khazanov
Writing – review & editing: Mike Chu, Marilia Samara, Robert G. Michell

© 2023. The Authors. Geophysical Research Letters published by Wiley Periodicals LLC on behalf of American Geophysical Union.
This is an open access article under the terms of the Creative Commons Attribution License, which permits use, distribution and reproduction in any medium, provided the original work is properly cited.

Abstract Wave-particle interaction processes in the equatorial magnetosphere initiate time-dependent electron precipitation in the pulsating aurora. These electrons enter loss-cone and bounce between the two magnetically conjugate hemispheres, collide with the atmospheric constituents, and introduce additional time scales in electron precipitation dynamics. In this letter we present preliminary results of pulsating aurora formation using the time-dependent SuperThermal Electron Transport code, which considers the magnetosphere-ionosphere-atmosphere energy coupling between the two magnetically conjugate regions and discuss their contribution to the peculiarities of electron distribution function formation within the pulsating aurora.

Plain Language Summary It is well known that pulsating aurora is caused by electrons coming from the magnetosphere that are modulated by electromagnetic waves. However, there is a complimentary process occurring that is little studied yet produces significant macroscopic effects. This process is the bouncing of electrons between the two magnetically conjugate regions which creates an additional important time scale for MIA coupling. In this letter, we describe using the time-dependent SuperThermal Electron Transport (STET) code to quantify the importance of this process in the temporal development of pulsating aurora by comparing to published optical observations, finding a remarkable agreement between the theoretical STET code predictions and those observed optically inside real aurora.

1. Introduction

Pulsating aurora is a type of diffuse aurora that has been well studied as demonstrated in several past review articles of Davidson (1990), Johnstone (1978), and Lessard (2012). The measured electron energies associated with pulsating aurora cover a large range, from as low as 1 keV (McEwan et al., 1981; Yau et al., 1981), 5–12 keV (Samara et al., 2015), to several tens of keV (Jaynes et al., 2013; Yau et al., 1981), and the temporal periods of the pulsations range from a few seconds to a few tens of seconds (e.g., Johnstone, 1978; Samara et al., 2017). Such a large range of energy and time-period variations is likely an indication of different generation mechanisms for the formation of pulsating aurora.

Wave-particle interaction (WPI) processes play the dominant role in the formation of pulsating and diffuse aurora (Miyoshi et al., 2013, 2015; Ni, Thorne, Horne, et al., 2011; Ni, Thorne, Meredith, et al., 2011; Thorne et al., 2010). Nishimura et al. (2010) suggested that chorus waves interact with equatorial electrons to produce pulsating auroras, while Mozer et al. (2017) examined the role of time domain structures in the formation of this phenomenon. Pioneering rocket-borne measurements of electron modulations within pulsating aurora by Yau et al. (1981) provided a clear indication that electrons of different energies were being injected with temporal variability from near the equatorial plane. All these potential scenarios of pulsating aurora driving are presented in Figure 1a; however, only chorus waves will be used in the model presented below.

Early in-situ measurements and theoretical work suggest that ∼10%–20% of the precipitated electron fluxes get reflected back to the conjugate hemisphere (O'Brien, 1964; Rees, 1968). Recently, Samara et al. (2017), for the first time, discussed a case study of a pulsating auroral event imaged optically at high time resolution and presented direct observational evidence in agreement with the interhemispheric electron bouncing at Poker Flat, AK. They also provided a semi-quantitative analysis of their measurements and found that these results are in the agreement with the SuperThermal Electron Transport (STET) model predictions (Khazanov et al., 2014, 2015).

uncorrected proof

10.1029/2023GL103019

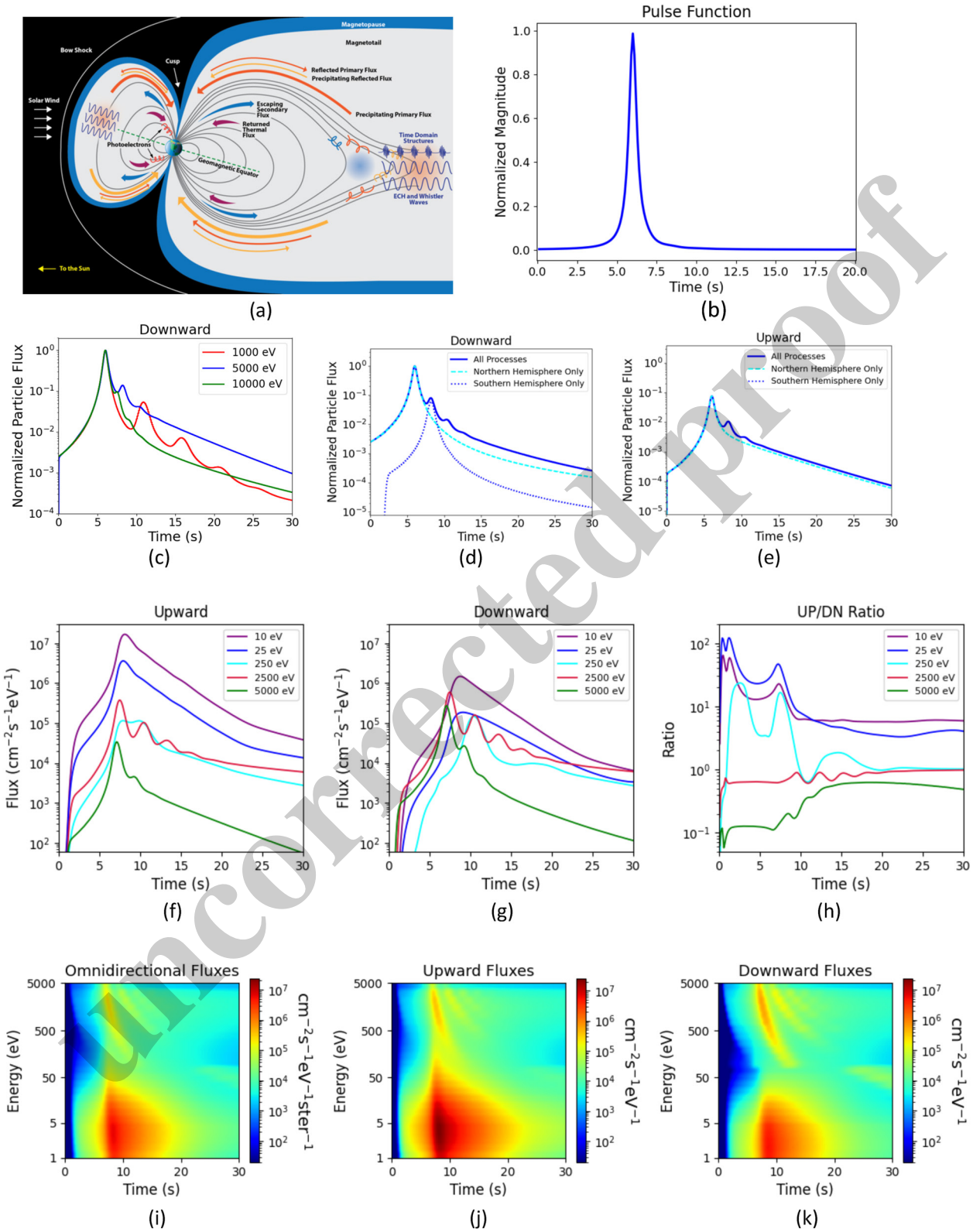

Figure 1. (a) Illustration of the magnetosphere-ionosphere-atmosphere coupling driving pulsating aurora; (b) the theoretical pulse function used in the SuperThermal Electron Transport (STET) simulation; (c) result for several monoenergetic electron particle fluxes from the STET simulation; (d–e) the 5 keV downward and upward electron fluxes calculated for the different STET scenarios in the magnetically conjugate points; (f–h) the behavior of the individual energies selected for display; (i–k) the entire energy spectra of precipitated electrons in the energy range of 1–5,000 eV.

uncorrected proof

The theoretical studies of aurora we mentioned above were focusing on the magnetospheric driver of electron precipitation into the atmosphere. However, as was suggested by Khazanov et al. (2017, 2021b), aurora is not only driven by pure magnetospheric processes. Magnetosphere-ionosphere-atmosphere (MIA) dynamics of the precipitating electrons and their coupling between the northern and southern hemispheres is also an extremely important mechanism in the formation of different kinds of auroras (Khazanov et al., 2020, 2021a). In this letter we continue to introduce MIA coupling physics of auroral electron precipitation phenomena and apply our study to pulsating aurora. The MIA energy coupling that produces electron pulsating aurora and other affiliated processes are shown in Figure 1a (adapted from Khazanov et al., 2020) and are elaborated below in the context of time-dependent studies of these phenomena using the STET code. To validate the theoretical approach in this paper for the analysis of pulsating auroral phenomena, we used the experimental results presented by Samara et al. (2017) and the newly developed non-steady state STET code that was employed in a manner similar to that recently applied to analyze the electron precipitation temporal dynamics during two substorms on 16 February 2010 (Khazanov et al., 2022).

2. The STET Code Setting

The Time-Dependent STET code to be used in this paper solves the gyro-average kinetic equation for SE for energies above 1 eV and is well documented (Khazanov, 2011; Khazanov et al., 2021a). Applying this kinetic equation for the SE in the pulsating aurora, can be presented as

$$\frac{1}{v}\frac{\partial \Phi}{\partial t} + \mu\frac{\partial \Phi}{\partial s} - \frac{1-\mu^2}{2}\left(\frac{1}{B}\frac{\partial B}{\partial s} - \frac{F}{E}\right)\frac{\partial \Phi}{\partial \mu} + EF\mu\frac{\partial}{\partial E}\left(\frac{\Phi}{E}\right) = \langle S\rangle, \tag{1}$$

where $\Phi = 2Ef/m^2$ is the SE flux in the units of $\mathrm{cm}^{-2}\ \mathrm{s}^{-1}\ \mathrm{eV}^{-1}\ \mathrm{ster}^{-1}$, v is SE velocity, t is time, s is the distance along the field line, E is the particle energy, and μ is the cosine of the pitch-angle. F is the electric field force, and $\langle S\rangle$, is a symbolic notation of collision integrals representing interactions of SE with thermal electrons and ions, scattering with neutral particles, and WPI. A detailed derivation of these collisional and WPI terms is given in Khazanov (2011) and Khazanov et al. (2015) and all are explicitly presented in Khazanov et al. (2020, 2021a).

In the model presented above, the time-dependent electron precipitation that initiates the pulsating aurora starts near the geomagnetic equator via interactions of whistler chorus waves with the trapped electron plasmasheet population. There are two primary ways to introduce time-dependent communication between the trapped plasmasheet electron population and those electrons that are in the loss-cone and precipitated: (a) Modulation of whistler waves by some lower frequency wave activity, (b) Steady-state whistler wave activity with a time variation of the communication between the trapped and loss-cone populations using an empirical time-dependent function. The latter is the most consistent with the observations presented by Yau et al. (1981).

Both approaches have uncertainties because neither the modulation nor the empirical time-dependent functions are explicitly known well enough. It should be noted that the primary focus of our study is the exploration of the role of MIA energy coupling in the formation of pulsating aurora. Therefore, the second communication scenario between the trapped and loss-cone populations was employed with a generalized trapped zone plasmasheet population described as:

$$\Phi_{\mathrm{trap}}(t, E) = T(t) * F(E) \tag{2}$$

The setting of Φ_{trap} and its communication with the solution of Equation 1 has been discussed in detail by Khazanov et al. (2015). The only difference here is the usage of a time dependent function, $T(t)$ and the selection of an arbitrary energy distribution function of $F(E)$ that is assumed to be isotropic for all energies in the STET simulations presented and specified below.

The results presented below use the following inputs from different independent models. The neutral atmospheric model used in the STET code is the MSIS-90 (Hedin, 1991). The plasma density structure in the ionosphere is based on the IRI-2016 model (Bilitza et al., 2017), and is extended into the magnetosphere as $N_e \sim B(s)^{3/2}$, where $B(s)$ is the magnetic field as the distance of s along the field line. Cross sections for elastic collisions, state-specific excitation and ionization were taken from Solomon et al. (1988).

The electron bounce time between the two magnetically conjugate regions introduces an additional time scale within the formation of pulsating aurora that has not been investigated in detail by previous analyses of this

uncorrected proof

phenomenon. Below we investigate how the time-dependent STET code represents electrons bouncing between the two magnetically conjugate regions, and how both regions contribute to the peculiarities of electron distribution function formation within the pulsating aurora. The major focus is given to the bouncing of auroral electrons with energies below 10 keV. This phenomenon, however, should occur at all energies. For example, it was recently reported to be present in microbursts with electron energies of 200–800 keV (Shumko et al., 2018). This paper does not consider any optical time-dependent emissions and assumes that the electron energy flux, the major focus of our analysis, is roughly proportional to the total optical intensity of the aurora (Stenbaek-Nielsen et al., 1998).

3. MIA Electron Bouncing Representation in the STET Code

To demonstrate the accuracy of the bounce-period analysis in STET code, we consider the monoenergetic electron flux bounces using the time function in Equation 2 as the pulse presented in Figure 1b by the following expression

$$T(t) = \frac{1}{1 + ((t - t_0)/W)^2} \tag{3}$$

with the following parameters: t_0 is the location of the peak and W is its width. For this study, the STET code sets t_0 at 6 s and W to be 0.3 s.

The monoenergetic electrons are driven by whistler mode chorus waves at a magnetospheric equatorial distance of $L = 5.9$. As in Khazanov et al. (2015), the intensities of the magnetic field for the lower band chorus (LBC) and upper band chorus (UBC) whistler waves were taken to be 100 pT^2 and they are within the range of the observed values presented by Meredith et al. (2009, 2012). We assumed that LBC waves are located within 15° of the magnetic equator, while UBC waves were within 10° (Ni, Thorne, Horne, et al., 2011; Ni, Thorne, Meredith, et al., 2011). The pitch angle diffusion coefficients for these waves were calculated as described in Khazanov et al. (2015).

These waves interact with the plasmasheet symmetrically, providing the identical electron precipitation into both magnetically conjugate hemispheres. Figure 1c displays several normalized monoenergetic electron particle fluxes that come to the northern hemisphere at the altitude of 800 km and bounce between the northern and southern footprints of the dipole magnetic field at an L-value of 5.9.

The biggest normalized particle flux spikes for all energies correspond to the initially injected electrons from the trapped population into the loss-cone via WPI processes, shown in Figure 1a as "Precipitating Primary Flux." The smaller spikes in Figure 1c show bouncing electron fluxes coming from magnetically conjugate regions. The second spikes represent electron fluxes injected to the southern hemisphere that backscattered to the northern hemisphere. The third spikes represent the electrons initially injected into the northern hemisphere that then bounced off the southern hemisphere and returned to the northern hemisphere. Additional diminishing spikes, as time develops, show the corresponding repeat-bouncing of the electrons.

As the electron energy increases, as seen in Figure 1c, the bouncing time between the northern and southern regions decreases, and the number of visible spikes is diminished. The latter effect is the result of deeper penetration into the atmosphere for the higher energy electrons, where they encounter more collisions and absorption.

To better represent the role of the bouncing processes of electrons in the pulsating aurora, Figures 1d and 1e show 5 keV downward and upward electron fluxes calculated for the different STET scenarios in the magnetically conjugate points. The solid lines in these figures represent the cases shown in Figure 1c, where all precipitation and scattering processes are taken into account in both magnetically conjugate hemispheres. The dashed and dotted lines in these figures represent the artificial STET case scenarios when southern or northern hemispheres are completely disconnected from the computation domain, correspondingly. These demonstrate that the bouncing processes are important elements in the formation of the pulsating aurora and must be taken into account in future theoretical studies of this phenomenon.

4. Electron Energy Spectra in Pulsating Aurora

Studying monoenergetic electron bouncing between the magnetically conjugate points presented above was an important element of our analysis that justifies properly calculated electron transit time in the STET code for the

uncorrected proof

$L = 5.9$ case. This will be further analyzed in the next section to explain the Poker Flat observation presented by Samara et al. (2017). However, in reality, electron precipitation that is driven by WPI processes at the geomagnetic equator can have broad energy spectra (Davidson, 1990; Johnstone, 1978; Lessard, 2012), and the final optical emissions that are observed in the pulsating aurora are driven by complicated time-dependent electron dynamics.

Now we modify the condition Equation 2 leaving $T(t)$ function as given by Equation 3 and presenting the Maxwellian energy distribution function of $F(E)$ as:

$$\Phi(E) = \mathrm{AEexp}\left(-\frac{E}{E_0}\right) \tag{4}$$

where E_0 and A are characteristic energy and normalization constant, that are selected to be 10^3 and 3,000 eV, correspondingly. As it was demonstrated by Khazanov et al. (2022), the STET code can operate with any arbitrary energy distribution function, and the selection of the function used in Equation 4 in this study is for illustration purposes. The choice of Equation 4 is also consistent with the observations presented by Yau et al. (1981).

Figures 1f–1h demonstrate the behavior of the individual energies, and Figures 1i–1k, and the entire energy spectra of precipitated electrons in the energy range of 1–5,000 eV. To begin with the initiation of Equation 2, the plasmasheet electron energy distribution function (Equation 4) was used only for energies of magnetospheric origin, chosen to be 100 to 5,000 eV (Khazanov et al., 2021b). Remarkably, even when using this wide range for the energy spectra of Equation 4, the individual energies at the altitude of 800 km, experiencing multiple bounces between the magnetically conjugate regions, show very clear bouncing spikes in downward (1f) and upward (1g) moving particle fluxes. The ratios between up and down moving electron fluxes presented in Figure 1h are very complicated with the tendency of the UP/DN ratio to increase as the energy decreases. These results are consistent with our previous analysis of the energy coupling in the region of the diffuse aurora (Khazanov et al., 2014, 2015) and FAST observations (Dombeck et al., 2018) in the corresponding auroral region. The higher energy range of the precipitated electrons continuously degrades toward the lower energies and produces the secondary electron populations. It contributes to the built up of lower energy spectra of precipitating electrons and the dominance of lower energy upward fluxes over their downward moving counterpart (Khazanov et al., 2021b).

The energy spectrograms in Figures 1i–1k also show time dependencies that are affiliated with electron bouncing between the two magnetically conjugate ionospheres. Because the optical emissions that are initiated by these precipitated electrons are proportional to their total energy fluxes, observers at the ground can see similar optical time dynamics as are shown in the time-dependent electron distribution function development presented in Figure 1k.

The STET code simulated results presented above were based on the pulse time function of Equation 3 that apparently corresponds the narrow packet of the chorus wave activity. Now let us move to the time function in Equation 2 that represents the broad wave activity band as shown in Figure 2a. It should be noted that our discussion regarding the narrow or the broad wave activity bands of the chorus waves is a speculative one, because we are not considering the specific wave-particle processes that lead to the generation of the time dependent structures like those shown in Figures 1b and 2a. This obstacle requires additional studies, but it does not contradict the general idea presented in our manuscript that studies the role of the interhemispheric electron bounce processes on the formation of the electron distribution functions within pulsating aurora.

We now consider a slightly longer magnetic field line at $L = 7$, leaving all waves and plasmasheet electron parameters unchanged. It should be noted, however, that further increase of the L-shell parameter could create significant non-dipole components of that magnetic field which is out of the scope of this manuscript. The simulation of pulsating aurora in our study is associated with time-dependent precipitating electron dynamics and require careful selection of integration time step in the solution of the kinetic Equation 1. Such a requirement is driven by multiple processes included in the STET code solution presented in our most recent studies (Khazanov et al., 2020, 2021b). Here, without going into the details of the numerical implementation of Equation 1, which is presented in the book by Khazanov (2011), we demonstrate the validity of our time step selection for the results presented here.

Figures 2b and 2c present the omnidirectional fluxes for the single energies calculated with different time steps, 0.01 and 0.1 s, for the numerical implementation of Equation 1. In all data presented in Figure 2, the plasmasheet

uncorrected proof

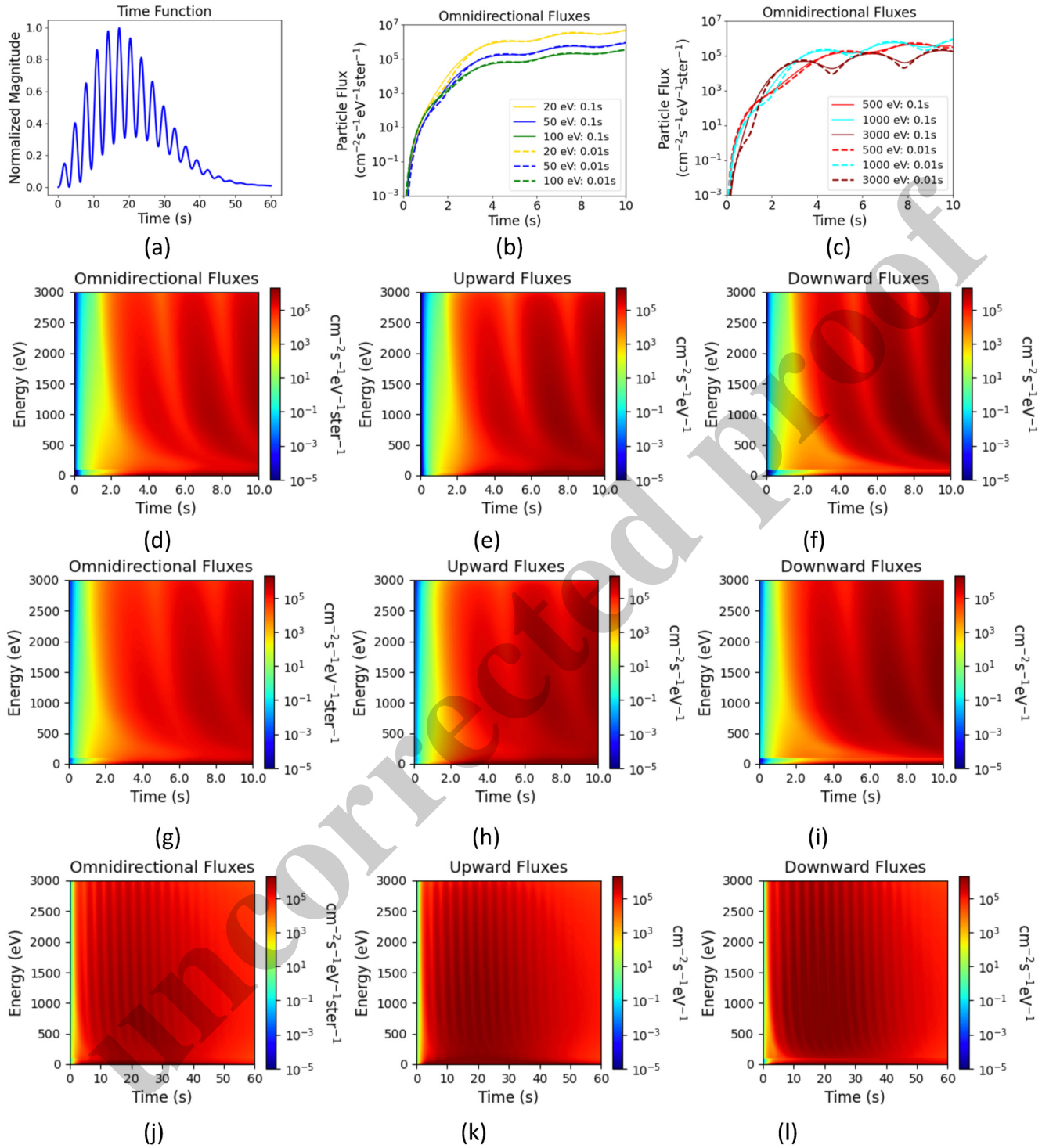

Uncorrected Proof

Figure 2. (a) The function representing the broad wave activity; (b–c) the omnidirectional fluxes for selected single energies calculated with timesteps of 0.01 and 0.1 s; (d–f) the electron energy spectra from the SuperThermal Electron Transport (STET) simulation using time step of 0.01 s; (g–i) the electron energy spectra from STET simulation using time step of 0.1 s; (j–l) the spectra for the 0.1 s timestep result up to 60 s.

electron energy distribution function was selected to be Equation 4 and to begin with including only electrons of magnetospheric origin from 100 to 3,000 eV (Khazanov et al., 2021b). The calculated energy spectra that are shown below correspond to the electron fluxes entering the upper ionospheric altitude of 800 km and include the electrons of ionospheric origin, secondary electrons, that are created via impact ionization in both magnetically

conjugate regions. This is consistent with statistical observations reported by Fukizawa et al. (2021) where they found electron density enhancements in the F-region associated with most pulsating auroral events and that nearly 90% of those observed were high enough in altitude that they would correspond to electrons that are less than 100 eV in energy. This is further evidence that secondary electrons of ionospheric origin are bouncing between the hemispheres in regions of pulsating aurora.

The electron energy spectra presented in Figures 2d–2f correspond to a STET simulation time step of 0.01 s, and Figures 2g–2i, to a time step of 0.1 s. The electrons with the single energies presented in Figures 2b and 2c were extracted from these electron energy spectra and demonstrate quantitative differences between the fluxes calculated using different time steps. The single energies above 100 eV have noticeable time variations that represent their bouncing between the northern and southern hemispheres. The corresponding time variations for the lower energies are gradually diminished (but still visible) because they are created at the ionospheric altitudes where electron collisional processes dominate over interhemispheric bouncing processes.

The further decrease of the integration time steps down to 0.001 s **does not change** the results presented in Figures 2b–2i to within less than 10%. However, if the time step is increased to 1 s (not shown here), the time-dependent bouncing structure of the electron energy spectra almost disappears. The empirical selection of the integration time step presented here requires at least 0.1 s to resolve the bouncing time scale that is visible on the simulated electron energy spectra. The electron energy spectra that are shown on the bottom row of Figure 2 demonstrate such a calculation up to 60 s.

5. Poker Flat Case Analysis

As we mention in the introduction to this manuscript, Samara et al. (2017), using auroral high time optical resolution instrumentation at Poker Flat, AK (geographic: 65.1°N, 147.4°W; geomagnetic: 65.7°N, 96.6°W; $L = 5.9$) location, presented direct first observational evidence of the interhemispheric electron bounces. We used these results in this section and applied the non-steady state STET code to verify its performance in this highly variable space plasma environment.

Figures 3a and 3b from that paper were used to set up the STET code simulation and for the subsequent verification of the theoretical results. Figure 3a shows the keogram extracted along a north-south cut through the optical images, covering 35 s of data. Figure 3b shows a time series of normalized emission intensity taken as an average of the keogram data in the vertical north-south direction. These data clearly show that immediately following each of the main pulsations there are fainter pulsations. These are interpreted as the electron bounce time between the hemispheres because they are spaced roughly equally regardless of the spacing between the main pulsations.

In order to further investigate the nature of the relationship between the primary and secondary peaks, the data from Figure 3b are shown expanded and annotated showing the consequent energy loses, corresponding peaks and the times between their arrival in the Poker Flat location. Assuming that the peaks in Figure 3b are caused by reflected electrons, and using the dipole magnetic field configuration, Samara et al. (2017) concluded that the travel times are estimated to be between 1.5 and 2.0 s, corresponding to 10–6 keV, respectively. These energies are consistent with the electron energies known to exist in pulsating aurora.

The specific wave environment in the magnetosphere during the experiment by Samara et al. (2017) is not known, therefore in setting up the STET code, we used the spacing between the primary peaks as presented by experimental data in Figures 3a and 3b. The narrow optical spikes in Figures 3a and 3b are believed to be affiliated with the narrow whistler wave band and the time function in Equation 2 should be represented by the pulse function (Equation 3) of Figure 1b. There are only three easily visible secondary peaks presented in Figures 3a and 3b. For the STET run, the energy range of the plasmasheet energy distribution function (Equation 4) was selected to be in the range of 8–10 keV. The electron energy spectrograms corresponding to this simulation are shown in Figures 3e–3g with the clear demonstration of electrons bouncing between hemispheres.

The large initial peaks presented in Figures 3a and 3b have clear separation in time and slightly different magnitudes. We ran STET code assuming that their magnitudes are identical, because the magnetospheric drivers are not known. We did use the observed separations in time between the larger peaks as presented by Samara et al. (2017). Because the STET kinetic Equation 1 is linear, the four peaks that are shown in Figure 3c were running independently and were separated in time identically with data in Figures 3a and 3b. Figure 3d represents

uncorrected proof

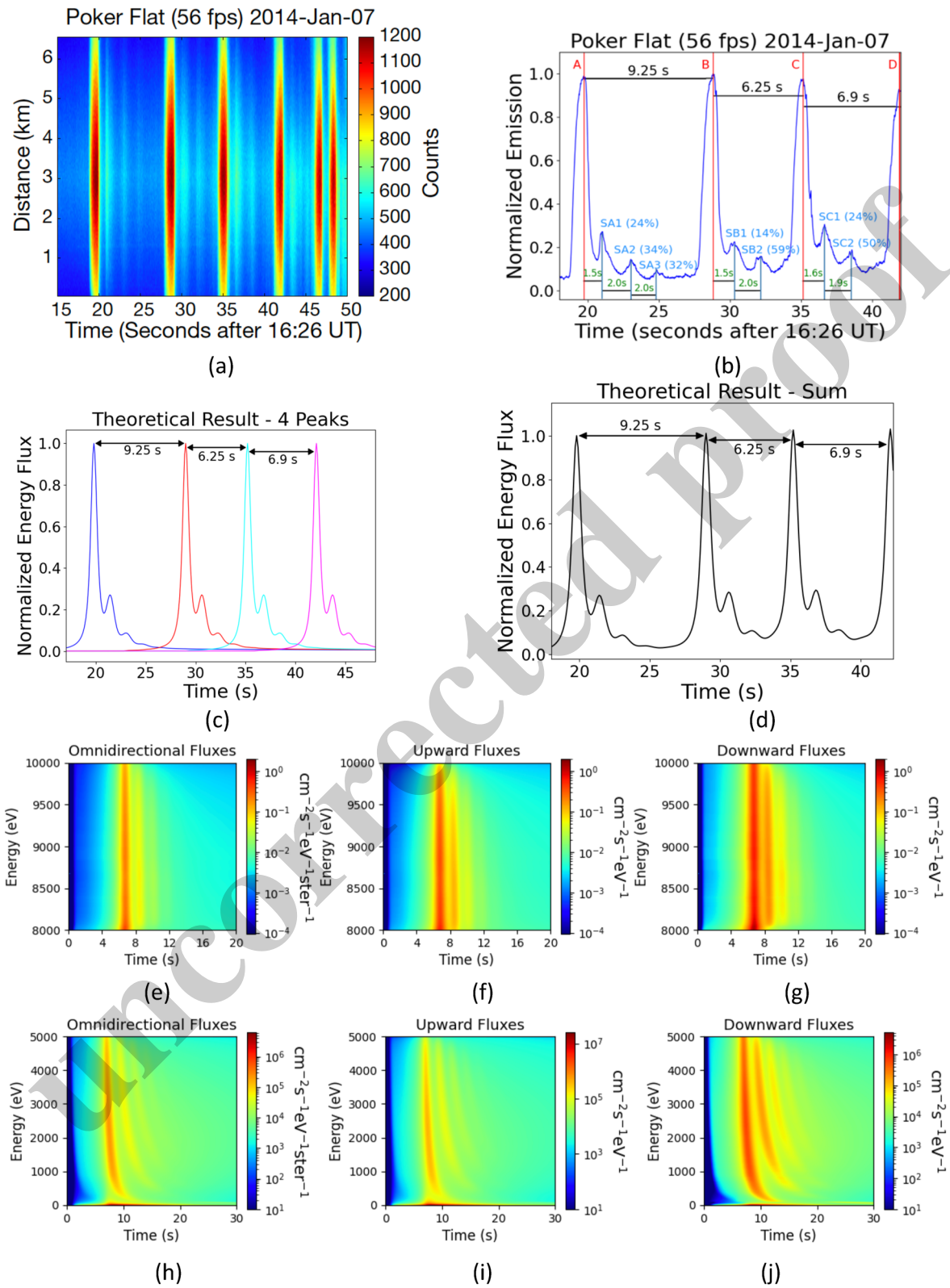

uncorrected proof

Figure 3. (a–b) Figures extracted from Samara et al. (2017) used to guide the SuperThermal Electron Transport (STET) code simulation; (c) the four peak functions independently simulated; (d) the summation of the four individual peak functions demonstrates a clear correspondence between observations and theoretical results; (e–f) the electron energy spectrogram in the energy range of 8,000–10,000 eV showing electrons bouncing between hemispheres; (h–j) demonstrate STET calculations covering energies of 1–5,000 eV showing clear signs of electron time dependencies in the energy range well below 1 keV.

the summation of Figure 3c results demonstrating a clear correspondence (within 10%–15%) between the observations (Figure 3b) and the theoretical results (Figure 3d), in terms of the times were these multiple secondary and tertiary peaks are located. This simulation result of four independently driven spikes highlights the communication between themselves, represented by the slight growth of their intensities at the bottoms of their origins, which is also clearly demonstrated in the observational data presented in Figure 3b. Moreover, the relative differences between the magnitudes of the large and small peaks, and their positions in time match remarkably well between the observational and simulated theoretical data.

The quantitative assessment of the role of atmospheric collisions in the simulation data presented above is in line with our previous studies (Khazanov et al., 2014, 2017, 2020, 2021a) and experimental results by Samara et al. (2017). Specifically, within the energy range of the pulsating aurora, 6–10 keV, about 14%–50% of the energy flux from the primary precipitating electrons gets reflected back up.

Most of the discussions regarding the analysis of different pulsating aurora events have focused on the auroral electrons in the keV energy range (e.g., Michell & Samara, 2015; Samara et al., 2017). Figures 3h–3j demonstrate STET calculations covering energies of 1–5,000 eV and we see the clear signs of electron time dependencies in the energy range well below 1 keV (also noted in the STET results of Figure 2). Optical features caused by electrons with energies of less than 1 keV are not observed to show significant temporal variations for two reasons. First, they typically do not contain enough total energy flux to create significant visible auroral structures. Second, they deposit their energy at higher altitudes where the Oxygen red line (630.0 nm) would be more predominantly produced. In addition, the red line has a long lived (110 s) excited state and therefore would not show any temporal variations on these shorter (few to 10 s) timescales.

6. Summary

Wave-particle interactions in the equatorial magnetosphere initiate time-dependent electron precipitation, causing pulsating aurora. A fraction of both the precipitating and secondary electrons are reflected upward toward the conjugate hemisphere. A subset of these upgoing electrons will bounce between the two magnetically conjugate hemispheres, collide with the atmospheric constituents, and introduce an additional time scale in the electron precipitation dynamics. In this letter we presented the preliminary results of the formation of the electron pulsating aurora, using the time-dependent STET code that considers MIA energy coupling between the two magnetically conjugate regions. Their contribution to the peculiarities of electron distribution function formation within the pulsating aurora is also discussed.

In this manuscript, we do not consider any optical time-dependent emissions generated by the STET code simulations and assume that the electron energy flux, the major focus of our analysis, is roughly proportional to the total optical intensity of the aurora (Stenbaek-Nielsen et al., 1998). In fact, these results show that the relative differences between the magnitudes of the primary and secondary peaks in the optical emissions are closely correlated with those in the precipitating electron energy flux, to within 15%–25% (Figures 3b–3d). Therefore, the assumption that the electron energy flux is proportional to the total optical intensity of the aurora is strongly validated by these results.

In the results presented above and shown in Figures 1–3, it was clearly demonstrated that electrons bounce between the two magnetically conjugate hemispheres and that they show some of the energy spectral features that demonstrate an additional time scale that must be taken into account in the analysis of the formation of pulsating aurora. Comparison of the optical observations by Samara et al. (2017) to STET code simulations, in particular, shows a remarkable agreement of the time scales as well as the relative magnitudes of the reflected electron flux features resulting from the electrons bouncing between hemispheres multiple times. This provides an additional validity for the usage of this code to study such a highly time-dependent phenomena as magnetic substorms (Khazanov et al., 2022).

Data Availability Statement

The STET code simulation data used to make some of the figures in this study are available at http://doi.org/10.5281/zenodo.7566034.

uncorrected proof

Acknowledgments
G. V. K. was supported by NASA HTMS program under award of 80NSSC20K1276, the MARBLE Project, funded by the NASA Living with a Star (LWS) Strategic Capabilities program, LWS Program under the award 80NSSC20K1817, NASA award 80NSSC21K1552 and the Comprehensive Auroral Precipitation Experiment (CAPE) on NASA's Geospace Dynamics Constellation (GDC) mission as part of the Living With a Star (LWS) program.

References

Bilitza, D., Altadill, D., Truhlik, V., Shubin, V., Galkin, I., Reinisch, B., & Huang, X. (2017). International reference ionosphere 2016: From ionospheric climate to real-time weather predictions. *Space Weather*, *15*(2), 418–429. https://doi.org/10.1002/2016SW001593

Davidson, G. T. (1990). Pitch-angle diffusion and the origin of temporal and spatial structures in morningside aurorae. *Space Science Reviews*, *53*(1–2), 45–82. https://doi.org/10.1007/bf00217428

Dombeck, J., Cattell, C., Prasad, N., Meeker, E., Hanson, E., & McFadden, J. (2018). Identification of auroral electron precipitation mechanism combinations and their relationships to net downgoing energy and number flux. *Journal of Geophysical Research: Space Physics*, *123*(12), 10064–10089. https://doi.org/10.1029/2018JA025749

Fukizawa, M., Sakanoi, T., Ogawa, Y., Tsuda, T. T., & Hosokawa, K. (2021). Statistical study of electron density enhancements in the ionospheric *F* region associated with pulsating auroras. *Journal of Geophysical Research: Space Physics*, *126*(12), e2021JA029601. https://doi.org/10.1029/2021JA029601

Hedin, A. E. (1991). Extension of the MSIS thermospheric model into the middle and lower atmosphere. *Journal of Geophysical Research*, *96*(A2), 1159–1172. https://doi.org/10.1029/90JA02125

Jaynes, A. N., Lessard, M. R., Rodriguez, J. V., Donovan, E., Loto'Aniu, T. M., & Rychert, K. (2013). Pulsating auroral electron flux modulations in the equatorial magnetosphere. *Journal of Geophysical Research: Space Physics*, *118*(8), 4884–4894. https://doi.org/10.1002/jgra.50434

Johnstone, A. D. (1978). Pulsating aurora. *Nature*, *274*(5667), 119–126. https://doi.org/10.1038/274119a0

Khazanov, G. V. (2011). *Kinetic theory of inner magnetospheric plasma* (pp. 372–584). Springer.

Khazanov, G. V., Gabrielse, C., Glocer, A., Chu, M., Nishimura, Y., & Reyes, P. (2022). A 2D kaleidoscope of electron heat fluxes driven by auroral electron precipitation. *Geophysical Research Letters*, *49*(18). https://doi.org/10.1029/2022gl100912

Khazanov, G. V., Glocer, A., & Chu, M. (2020). The formation of electron heat flux in the region of diffuse aurora. *Journal of Geophysical Research: Space Physics*, *125*(8). https://doi.org/10.1029/2020ja028175

Khazanov, G. V., Glocer, A., & Chu, M. (2021a). Electron energy interplay in the geomagnetic trap below the auroral acceleration region. *Journal of Geophysical Research: Space Physics*, *126*(5). https://doi.org/10.1029/2020ja028811

Khazanov, G. V., Glocer, A., & Chu, M. (2021b). The precipitated electrons in the region of diffuse aurora driven by ionosphere-thermosphere collisional processes. *Geophysical Research Letters*, *48*(16), e2021GL094583. https://doi.org/10.1029/2021gl094583

Khazanov, G. V., Glocer, A., & Himwich, E. W. (2014). Magnetosphere-ionosphere energy interchange in the electron diffuse aurora. *Journal of Geophysical Research: Space Physics*, *119*(1), 171–184. https://doi.org/10.1002/2013JA019325

Khazanov, G. V., Sibeck, D. G., & Zesta, E. (2017). Is diffuse aurora driven from above or below? *Geophysical Research Letters*, *44*(2), 641–647. https://doi.org/10.1002/2016gl072063

Khazanov, G. V., Tripathi, A. K., Sibeck, D., Himwich, E., Glocer, A., & Singhal, R. P. (2015). Electron distribution function formation in regions of diffuse aurora. *Journal of Geophysical Research: Space Physics*, *120*(11), 1–25. https://doi.org/10.1002/2015JA021728

Lessard, M. R. (2012). A review of pulsating aurora. In A. Keiling, et al. (Ed.), *Auroral phenomenology and magnetospheric processes: Earth and other planets*. *Geophys. Monogr. Ser*. (pp. 55–68) (Vol. 197). AGU. https://doi.org/10.1029/2011GM001187

Li, W., Ni, B., Thorne, R. M., Bortnik, J., Green, J. C., Kletzing, C. A., et al. (2013). Constructing the global distribution of chorus wave intensity using measurements of electrons by the POES satellites and waves by the Van Allen Probes. *Geophysical Research Letters*, *40*(17), 4526–4532. https://doi.org/10.1002/grl.50920

McEwan, D. J., Yee, E., Whalen, B. A., & Yau, A. W. (1981). Electron energy measurements in pulsating aurora. *Canadian Journal of Physics*, *50*, 1106–1115.

Meredith, N. P., Horne, R. B., Sicard-Piet, A., Boscher, D., Yearby, K. H., Li, W., & Thorne, R. M. (2012). Global model of lower band and upper band chorus from multiple satellite observations. *Journal of Geophysical Research*, *117*(A10), A10225. https://doi.org/10.1029/2012JA017978

Meredith, N. P., Horne, R. B., Thorne, R. M., & Anderson, R. R. (2009). Survey of upper band chorus and ECH waves: Implications for the diffuse aurora. *Journal of Geophysical Research*, *114*(A7), A07218. https://doi.org/10.1029/2009JA014230

Michell, R. G., & Samara, M. (2015). Groundmagnetic field fluctuations associated with pulsating aurora. *Journal of Geophysical Research: Space Physics*, *120*(10), 9192–9201. https://doi.org/10.1002/2015JA021252

Miyoshi, Y., Saito, S., Seki, K., Nishiyama, T., Kataoka, R., Asamura, K., et al. (2015). Relation between fine structure of energy spectra for pulsating aurora electrons and frequency spectra of whistler mode chorus waves. *Journal of Geophysical Research: Space Physics*, *120*(9), 7728–7736. https://doi.org/10.1002/2015JA021562

Mozer, F. S., Agapitov, O. V., Hull, A., Lejosne, S., & Vasko, I. Y. (2017). Pulsating auroras produced by interactions of electrons and time domain structures. *Journal of Geophysical Research: Space Physics*, *122*(8), 8604–8616. https://doi.org/10.1002/2017JA024223

Ni, B., Thorne, R. M., Horne, R. B., Meredith, N. P., Shprits, Y. Y., Chen, L., & Li, W. (2011). Resonant scattering of plasma sheet electrons leading to diffuse auroral precipitation: 1. Evaluation for electrostatic electron cyclotron harmonic waves. *Journal of Geophysical Research*, *116*(A4), A04218. https://doi.org/10.1029/2010JA016232

Ni, B., Thorne, R. M., Meredith, N. P., Horne, R. B., & Shprits, Y. Y. (2011). Resonant scattering of plasma sheet electrons leading to diffuse auroral precipitation: 2. Evaluation for whistler mode chorus waves. *Journal of Geophysical Research*, *116*(A4), A04219. https://doi.org/10.1029/2010JA016233

Nishimura, Y., Bortnik, J., Li, W., Thorne, R. M., Lyons, L. R., Angelopoulos, V., et al. (2010). Identifying the driver of pulsating aurora. *Science*, *330*(6000), 81–84. https://doi.org/10.1126/science.1193186

O'Brien, B. J. (1964). High-latitude geophysical studies with satellite Injun 3: 3. Precipitation of electrons into the atmosphere. *Journal of Geophysical Research*, *69*(1), 13–43. https://doi.org/10.1029/JZ069i001p00013

Rees, M. H. (1968). Conjugate effects of atmospherically scattered auroral electrons. *Radio Science*, *3*(7), 645–649. https://doi.org/10.1002/rds196837645

Samara, M., Michell, R. G., & Khazanov, G. V. (2017). First optical observations of interhemispheric electron reflections within pulsating aurora. *Geophysical Research Letters*, *44*(6), 2618–2623. https://doi.org/10.1002/2017GL072794

Samara, M., Michell, R. G., & Redmon, R. J. (2015). Low-altitude satellite measurements of pulsating auroral electrons. *Journal of Geophysical Research: Space Physics*, *120*(9), 8111–8124. https://doi.org/10.1002/2015JA021292

Shumko, M., Sample, J., Johnson, A., Blake, J. B., Crew, A. B., Spence, H. E., et al. (2018). Microburst scale size derived from multiple bounces of a microburst simultaneously observed with the FIREBIRD-II CubeSats. *Geophysical Research Letters*, *45*(17), 8811–8818. https://doi.org/10.1029/2018GL078925

Solomon, S., Hays, P., & Abreu, V. (1988). The auroral 6300. Emission: Observations and modeling. *Journal of Geophysical Research*, *93*(A9), 9867–9882. https://doi.org/10.1029/JA093iA09p09867

uncorrected proof

Stenbaek-Nielsen, H. C., Hallinan, T. J., Osborne, D. L., Kimball, J., Chaston, C., McFadden, J., et al. (1998). Aircraft observations conjugate to FAST: Auroral are thicknesses. *Geophysical Research Letters*, *25*(12), 2073–2076. https://doi.org/10.1029/98GL01058

Thorne, R. M., Ni, B., Tao, X., Horne, R. B., & Meredith, N. P. (2010). Scattering by chorus waves as the dominant cause of diffuse auroral precipitation. *Nature*, *467*(7318), 943–946. https://doi.org/10.1038/nature09467

Yau, A. W., Whalen, B. A., & McEwen, D. J. (1981). Rocket-borne measurements of particle pulsation in pulsating aurora. *Journal of Geophysical Research*, *86*(A7), 5673–5681. https://doi.org/10.1029/JA086iA07p05673

uncorrected proof